Journal of Hazardous Materials 186 (2011) 1503–1512

Contents lists available at ScienceDirect

Journal of Hazardous Materials

journal homepage: www.elsevier.com/locate/jhazmat

Analytical expressions for predicting performance of aerosol filtration media made up of trilobal fibers

S. Fotovati [a], H. Vahedi Tafreshi [a,*], B. Pourdeyhimi [b]

[a] Mechanical Engineering Department, Virginia Commonwealth University, Richmond, VA 23284-3015, United States
[b] Nonwovens Cooperative Research Center, The Nonwovens Institute, NC State University, Raleigh, NC 27695-8301, United States

ARTICLE INFO

Article history:
Received 16 May 2010
Received in revised form 30 August 2010
Accepted 7 December 2010
Available online 15 December 2010

Keywords:
Aerosol filtration
Trilobal fibers
CFD simulation

ABSTRACT

Despite the widespread use of fibrous filtration media made up of trilobal fibers (referred to as trilobal media here), no mathematical formulations have yet been developed to predict their collection efficiency or pressure drop. In this study, we model the cross-section of a trilobal fiber with three overlapping ellipses separated from one another by a 120° transformation. We generate 2-D models representing the internal structure of trilobal filters having fibers with different dimensions and aspect ratios, and used them to predict pressure drop and collection efficiency of trilobal filter media. This information is then utilized to define an equivalent medium with circular fibers for each trilobal filter. Our results indicate that the circumscribed circle of a trilobal fiber can serve as an equivalent circular diameter, and therefore be used in the existing empirical/semi-empirical correlations that have previously been developed for predicting performance of filters with circular fibers. We have also proposed easy-to-use expressions that can be used with our equivalent circumscribed diameters for calculating the pressure drop of trilobal media.

© 2010 Elsevier B.V. All rights reserved.

1. Introduction

Fibers with trilobal cross-sections are currently used for air and water filtration in variety of applications [1–3]. An example of such media is a family of Spun-bonded Polyester fibers produced by BBA Fiberweb and sold under the brand name REEMAY. Since the infancy of filtration theory, about fifty years ago, fibers have been assumed to have circular cross-sections. There are many analytical, numerical, and empirical correlations available for predicting the collection efficiency and pressure drop of fibrous media made of fibers with circular cross-sections (referred to as *circular media* here for brevity). Our extensive literature search resulted only in a very few studies reporting filtration performance of media with trilobal fibers (referred to as *trilobal media* here for brevity). This includes the experimental studies of Lamb and Costanza [2], and Sanchez et al. [3], as well as the numerical simulations of Raynor and Kim [4]. To the knowledge of the authors, however, no analytical expressions have yet been proposed for predicting the performance of filters with trilobal fibers. Our objective in this paper is to establish simple analytical expressions that allow investigators to predict collection efficiency and pressured drop for their trilobal fibrous filters. We will also discuss and compare the performance of filters made of trilobal fibers with their equivalent media made of circular fibers. In particular, we conduct a series of computational fluid dynamics (CFD) simulations to determine an equivalent circular fiber diameter, thereby taking advantage of the existing expressions developed in the past for filters with circular fibers.

In the next section, we present a brief summary of the popular expressions available for predicting performance of filters with circular fibers. This is followed by our geometrical representation of trilobal cross-sections in Section 3. Fluid flow governing equations, particle trajectory formulations, and further details about the simulations are presented in Section 4. In Section 5, we present our results and discussion. This is followed by Section 6 where we compare findings of our 2-D simulations, obtained by enhancing the Fluent CFD code, with the 3-D simulation results obtained using FilterDict software (www.geodict.com) for verifications. Summary of the work and our conclusions are presented in Section 7.

2. Aerosol filtration via filters with circular fibers

There are various expressions that have been developed for predicting pressure drop and collection efficiency of media with circular fibers (see [5] for a review). In almost all these models, pressure drop across a medium is presented as a function of fiber diameter d_f and Solid Volume Fraction (SVF) α:

$$\frac{\Delta p}{t} = f(\alpha)\frac{4\mu U}{d_f^2} \quad (1)$$

* Corresponding author. Tel.: +1 804 828 9936; fax: +1 804 827 7030.
E-mail address: htafreshi@vcu.edu (H.V. Tafreshi).

0304-3894/$ – see front matter © 2010 Elsevier B.V. All rights reserved.
doi:10.1016/j.jhazmat.2010.12.027

Nomenclature

a	ellipse major axis length
b	ellipse minor axis length
e	eccentricity
s	trilobal surface area
C_c	cunningham slip correction factor
D	diffusivity
d_f	fibers diameter
d_p	particle diameter
E	total filter efficiency
E_D	single fiber efficiency due to diffusion
E_R	single fiber efficiency due to interception
E_I	single fiber efficiency due to inertial impaction
$f(\alpha)$	dimensionless pressure drop
h	height of the domain
N_p	particle density per unit length
Ku	Kuwabara number
K_t	ratio of SVF of equivalent circular medium and trilobal medium
n	particles concentration
P	penetration
p	pressure
Pe	peclet number
R	particle to fiber diameter ratio
Stk	stokes number
T	temperature
t	filter thickness
U	face velocity
u	velocity in the x-direction
V	face velocity
v	velocity in the y-direction
v_{ip}	particle respective velocity in the both x and y direction

Greek letters

α	Solid Volume Fraction (SVF)
μ	Air viscosity
σ	Boltzmann constant
ζ	Major to minor axis length ratio for ellipse

where μ and U are the fluid viscosity and flow face velocity, respectively, and t is the filter thickness. Here we use an expression for $f(\alpha)$ proposed by Drummond and Tahir [6] as:

$$f(\alpha) = \frac{8\alpha}{-\ln \alpha - 1.476 + 2\alpha - 1.774\alpha^2} \tag{2}$$

For very small particles, capture is mainly due to the Brownian diffusion. Single fiber capture efficiency due to Brownian diffusion is given as [7]:

$$E_D = 2.9Ku^{-1/3}Pe^{-2/3} + 0.62Pe^{-1} \tag{3}$$

where Ku is the Kuwabara factor $Ku = -0.5\ln\alpha - 0.75 + \alpha - 0.25\alpha^2$ and Pe is the Peclet number $Pe = Ud_f/D$. Here $D = \sigma C_C T/(3\pi\mu d_P)$ is the diffusivity, and $\sigma = 1.38 \times 10^{-23}\,(\mathrm{m^2 kg\,s^{-2}\,K^{-1}})$ is the Boltzmann constant. T and μ are the air temperature and viscosity, respectively, and d_p is the particle diameter. For larger particles, where the size and mass of the particles are not negligible, filtration is due to interception and inertial impaction. Collection efficiency due to interception is given as [8]:

$$E_R = \frac{1+R}{2Ku}\left[2\ln(1+R) - 1 + \alpha + \left(\frac{1}{1+R}\right)^2\left(1-\frac{\alpha}{2}\right) - \frac{\alpha}{2}(1+R)^2\right] \tag{4}$$

where

$$R = \frac{d_p}{d_f}. \tag{5}$$

Collection efficiency due to inertial impaction is given as [9]:

$$E_I = \frac{(Stk)J}{(2\,Ku)^2} \tag{6}$$

where $Stk = \rho_P d_P^2 C_C V/18\mu d_f$ is the Stokes number and $J = (29.6 - 28\alpha^{0.62})R^2 - 27.5R^{2.8}$ while the equation is valid for $R < 0.4$.

Interception and inertial impaction play negligible roles in capturing very small particles. On the other hand, for particles larger than 500 nm at normal temperatures and pressures, Brownian diffusion is practically non-existent, and the collection efficiency is due solely to interception and inertial impaction. In this work, we consider Brownian diffusion for particles up to 500 nm in diameter.

Particle penetration through a fibrous filter with a thickness of t can be obtained by [10]:

$$P = \exp\left(\frac{-4\alpha E t}{\pi d_f(1-\alpha)}\right) \tag{7}$$

where E is the total single fiber efficiency defined as:

$$E = 1 - (1-E_D)(1-E_R)(1-E_I) \tag{8}$$

3. Equivalent circular fiber diameter for trilobal fibers

Expressions given in Section 2 are defined for medium with circular fibers. There are no such relationships for trilobal media; trial-and-error has been the only possible method for developing trilobal media. A widely accepted, but not documented, notion among the practitioners has been to consider an equivalent circular fiber that has the same cross-sectional area as the trilobal fibers, and use it in the equations given in Section 2. Our objective here is to firstly determine whether or not such an area-based equivalent fiber diameter definition is accurate, and if not, propose an alternative definition.

Fig. 1a shows an example of a fibrous filter with trilobal fibers used for particle filtration. Trilobal fibers are often produced by forcing a polymer through Y-shaped slots [11], and the final geometry of the fiber does not have a specific mathematical description. Therefore, we approximated these geometries with three overlapping ellipses (see Fig. 1b). To generate a trilobal cross-section, we rotated an ellipse about its antipodal point by 120° and 240°, and united the resulting ellipses with one another. Considering an ellipse along the x-axis, we have:

$$b^2(x - x_0)^2 + a^2y^2 = a^2b^2 \tag{9}$$

where a and b are lengths of the ellipse's major and minor axes, respectively, $x_0 = a(1+e)$ is the x-coordinate of the ellipse's center, and $e = \sqrt{1-(b/a)^2}$ is its eccentricity. After a θ° rotation about the antipodal point, we obtain:

$$b^2(x\cos\theta - x_0 + y\sin\theta)^2 + a^2(y\cos\theta - x\sin\theta)^2 = a^2b^2 \tag{10}$$

It is now easy to find the coordinates of the intersection points between the above ellipses and use them to calculate the perimeter of the trilobal cross-section. For the perimeter calculations, we represent the original ellipse in parametric form, i.e., $\vec{r}(\theta) = [a\cos\theta,\ b\sin\theta]$ and calculated the length of the arc from point D to point A (corresponding to θ_D and θ_A, respectively). The perimeter, p, of the trilobal geometry is then:

$$p = 6\int_{\theta_D}^{\theta_A} \sqrt{\vec{r}'(\theta)\cdot\vec{r}'(\theta)}\,d\theta \tag{11}$$

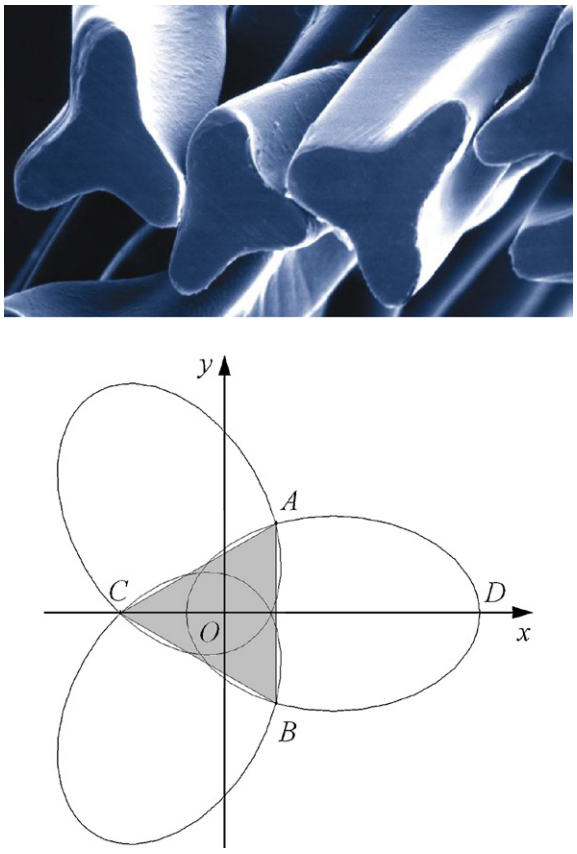

Fig. 1. (a) Trilobal fiber, *Source*: http://www.fiberwebfiltration.com/Reemay.cfm, (b) overlapping ellipses forming a trilobal cross-section.

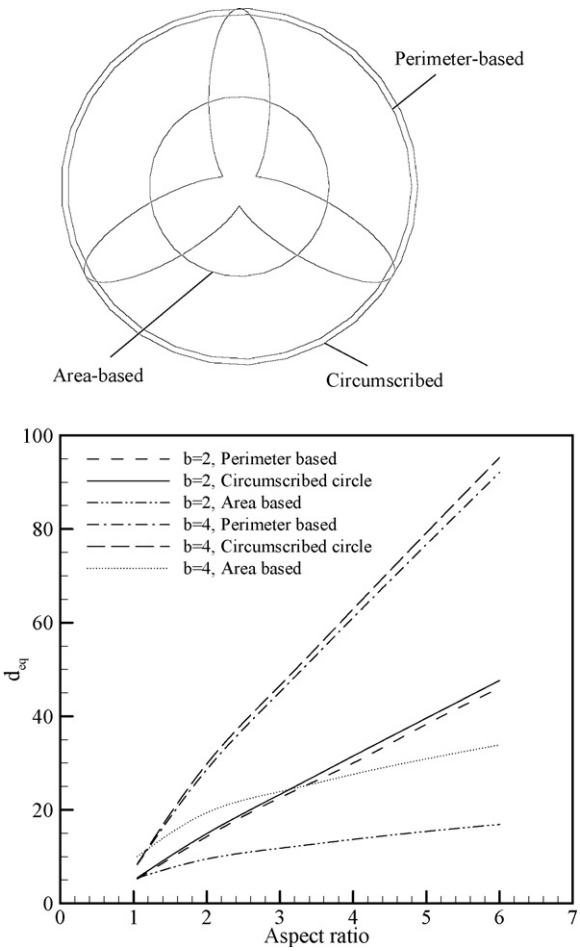

Fig. 2. Equivalent circular diameters obtained based on equal surface area and equal perimeter are compared with the diameter of the circumscribed circle for trilobal fibers with different aspect ratios and two different minor axes of $b = 2$ and 4 μm. It can be seen that equivalent diameter based on equal perimeter is very close to the diameter of the circumscribed circle.

where $\vec{r}'(\theta) = d\vec{r}/d\theta$. To find the surface area of the trilobal cross-sections, we considered the original ellipse and calculated the surface area under the arc from point D to point A (corresponding to x_D and x_A, respectively). Therefore,

$$s - s_t = 6 \int_{x_D}^{x_A} b\sqrt{1 - \frac{(x - x_0)^2}{a^2}}\,dx \tag{12}$$

where s and s_t are the surface area of the trilobal cross-sections and the triangular area formed between the three intersection points (shown in grey in Fig. 1b), respectively. Knowing the coordinates of the intersection points A, B, and C, the surface area of this equilateral triangle can easily be calculated:

$$s_t = \frac{1}{2}\sin\frac{\pi}{3}((x_A - x_B)^2 + (y_A - y_B)^2) \tag{13}$$

Knowing s and p, we can then define equivalent circular geometries having identical areas or perimeters as the trilobal cross-sections and determine the accuracy of such equivalent diameter definitions in predicting pressure drop and collection efficiency of trilobal media. Here, we also define an equivalent diameter based on the trilobal cross-section's circumscribed circle and used it in performance prediction.

Fig. 2 compares equivalent circular diameters obtained for trilobal cross-sections having different size and aspect ratios, $\zeta = a/b$. These calculations indicate that equivalent diameters based on the perimeter and circumscribed circle are almost identical. Therefore, we only use circumscribed circles in the rest of this paper and compare them with the area-based diameter definition.

4. Governing equations

In this section, we present the 2-D governing equations for aerosol flows. The air flow through the microstructure of a filter is believed to be governed by the Stokes equation, where the pressure drop is caused solely by viscous forces. Conservation of mass and momentum are given as:

$$\frac{\partial u}{\partial x} + \frac{\partial v}{\partial y} = 0 \tag{14}$$

$$\frac{\partial p}{\partial x} = \mu\left(\frac{\partial^2 u}{\partial x^2} + \frac{\partial^2 u}{\partial y^2}\right) \tag{15}$$

$$\frac{\partial p}{\partial y} = \mu\left(\frac{\partial^2 v}{\partial x^2} + \frac{\partial^2 v}{\partial y^2}\right) \tag{16}$$

For small airborne particles, we considered a convective-diffusive equation for the concentration of the particles based on the Eulerian approach [12]:

$$u\frac{\partial n}{\partial x} + v\frac{\partial n}{\partial y} = D\left(\frac{\partial^2 n}{\partial x^2} + \frac{\partial^2 n}{\partial y^2}\right) \tag{17}$$

where n is the nanoparticle concentration. Eqs. (14)–(16) are numerically solved in a series of 2-D geometries using the Computational Fluid Dynamics (CFD) code from Fluent Inc. (Fluent 6.3). We used the SIMPLE algorithm for pressure-velocity coupling along

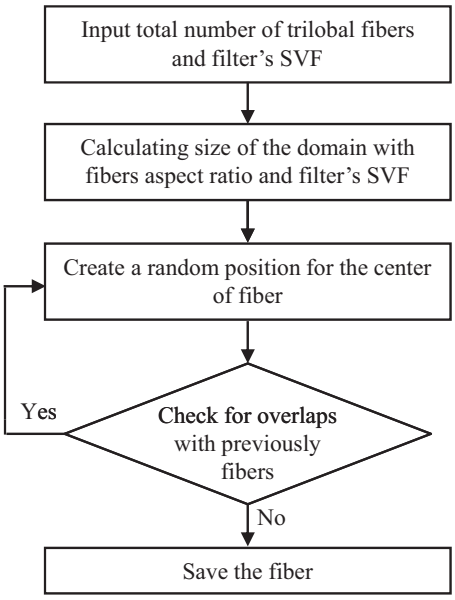

Fig. 3. Our program's flowchart for generating media with random trilobal fibers.

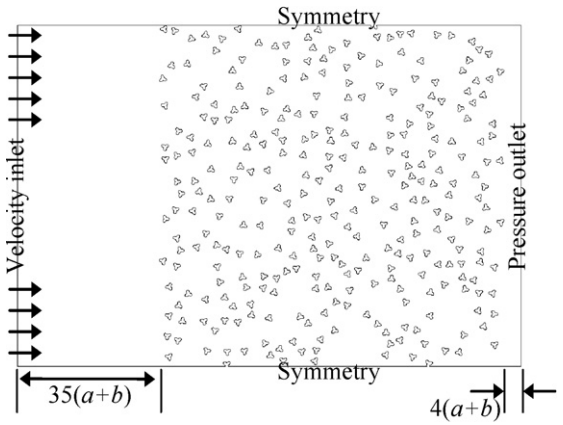

Fig. 4. An example of our simulation domains consisting of 300 trilobal fibers with an aspect ratio of 1.5 randomly placed in a square domain, resulting in an SVF of 10%. Inlet and outlet zones are considered up and downstream of the filter medium to accurately calculate pressure drop and particle collection efficiency.

with a second order upwind scheme for the momentum equation discretization. Eq. (17) is the conservation of mass (nanoparticles), and is introduced to the Fluent solver via a User-Defined Function (UDF). Fluent software solves this new equation inside the domain along with conservation of mass and momentum. The boundary conditions for the additional equation also need to be set as explained later in this section.

Our criterion for convergence was at least four orders of magnitude reduction in the residuals for the continuity and momentum equations in the x and y directions. More importantly, we monitored the pressure drop across the media during the iterations, in order to ensure that no significant changes occur in the flow field calculation upon performing further iterations when a simulation is considered converged.

For larger particles ($d_P \geq 100$ nm), we used a Lagrangian modeling approach where each individual particle is tracked throughout the solution domain. In the Lagrangian method, the force balance on a given particle is integrated to obtain the particle position in time. The dominant force acting on a particle is the air drag force. For $\mathrm{Re}_p = \rho V d_p/\mu < 1$ [13]:

$$\frac{dv_i}{dt} = \frac{18\mu}{d_p^2 \rho_p C_c}(v_i - v_i) \tag{18}$$

where v_i and v_{ip} are the respective field and particle velocity in the x or y direction.

To generate 2-D random fibrous geometries, a FORTRAN computer program was developed to produce fibrous structures of different porosities and thicknesses. The media generation process is explained in the flow chart shown in Fig. 3. Trilobal fibers are treated as circles with a diameter equal to that of their circumscribed circle and are randomly placed in a square domain. The media generation starts by sequentially adding the fibers into a square domain with a size obtained from SVF and the number of fibers considered for the simulations. Distance between a new fiber and the existing ones are continuously monitored to avoid fiber–fiber overlaps. Moreover, to ensure that a high-quality mesh can be generated inside the domain, fibers were not permitted to touch one another. Therefore, a minimum gap of $1.2d_{cc}$ was enforced between the fibers' center-to-center distance (d_{cc} is the diameter of the circumscribed circle). Note that this is just a simplification considered in this study, as the fibers do touch one another in a real filter medium. However, the impact of crossover points (fiber-to-fiber contact points) on the pressure drop and collection efficiency of a filter medium is quite negligible at porosities as high as those considered in this paper (more than 90%) and in the absence of particle caking. More information regarding the effects of fiber-to-fiber contact can be found in our previous publications [14–16]. A similar approach has also been used by Wang and Pui [17], Raynor [18], and Regan and Raynor [19].

At the end of the media generation process, the geometry is exported to Gambit software (a preprocessor for Fluent CFD code) via a script file for meshing. The mesh files were then exported to Fluent for finite volume calculations. Fig. 4 shows an example of a 2-D random fibrous medium with a thickness of 380 μm and a SVF of 10%, consisting of 300 trilobal fibers, having a minor axis of 2 μm, and an aspect ratio of 1.5.

Simulation boundary conditions are shown in Fig. 4. Uniform velocity and concentration profiles are assumed for the incoming airborne particles at the inlet. It is assumed here that particles that come in contact with the fibers will be captured and vanish from the solution domain. Note that the inlet and outlet boundaries are placed far up and downstream, so that a uniform flow can be assumed to prevail at the inlet and outlet [20,21]. We used an upstream distance of $L = 35(a+b)$ for our small particle (Eulerian) and large particle (Lagrangian) flow simulations, respectively, to improve the calculation's accuracy. For the case of small particles (Eq. (17)), we assumed $n = 0$ at the fiber surface and $\partial n/\partial x = 0$ at the outlet (no change in the particle concentration flux at the outlet). Our outlet boundary is placed at a distance of $4(a+b)$ downstream of the filter. We did not observe any significant errors caused by the above $4(a+b)$ distance. However, it is advisable to place such zero-streamwise gradient boundaries far downstream of the filter to ensure that the simulations converge to accurate values.

As the fibers are randomly distributed in the simulation domain, it is always necessary to repeat each simulation a number of times and average the results. It is also important to ensure that the domain size considered for the simulations is large enough so that the results are not affected by any size-related artifact. The larger the domain size, the fewer the number of required repetitions for smoothing out the statistical fluctuation of the results. In this study, we considered 300 fibers in our simulations domains and repeated each simulation 3 to 5 times.

Symmetry boundary conditions are considered for the upper and lower boundaries of the domain, i.e., the gradient of flow properties (velocity, particle concentration, etc.) is zero at these boundaries. The general problem with symmetry boundary condi-

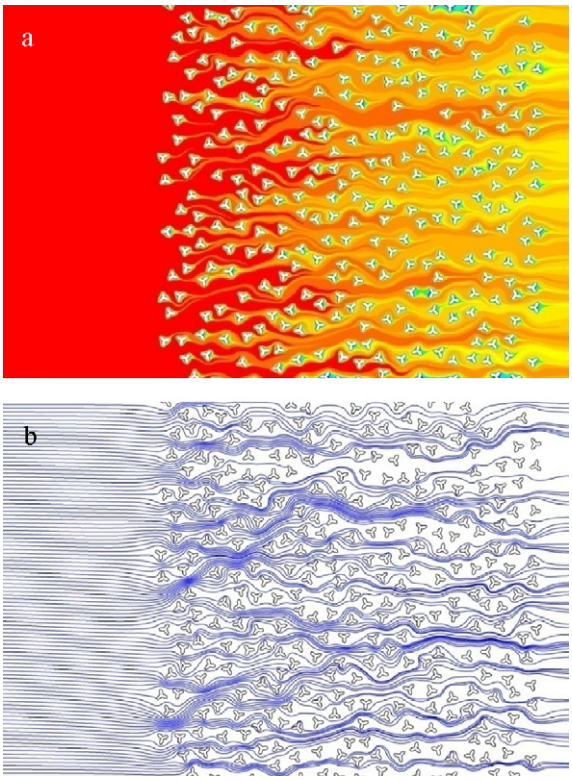

Fig. 5. Contours of normalized nanoparticle concentration are shown in a trilobal medium with an SVF of 10% consisting of fibers with an aspect ratio of 2 (a). Few particle trajectories are shown to demonstrate particle collection due to interception (b).

tion is that it does not allow lateral flow to take place. However, for large simulation domains, like those considered here, this should not be a concern as the net flow in the lateral directions will average to zero.

Standard Discrete Phase Model (DPM) in the Fluent code ignores the dimensions of the particle during trajectory tracking. A collision between a particle and a wall boundary is considered to be the moment that the particle center of mass touches the wall boundary, which obviously is not realistic. In this work, we developed a UDF to instruct Fluent to stop the particle if it comes in one radius

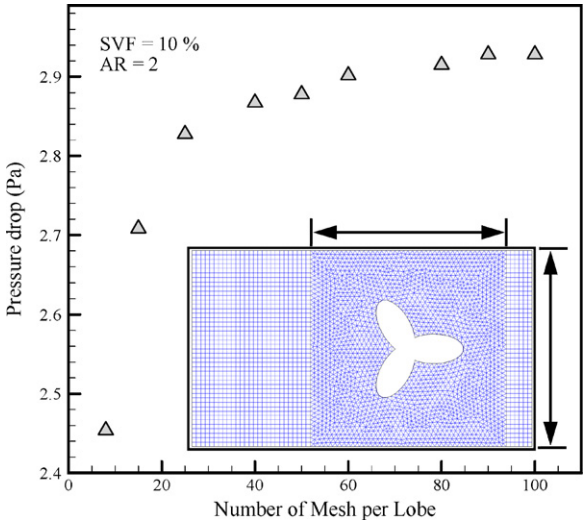

Fig. 6. Influence of grid density on the pressure drop caused by a single fiber placed in a domain with an SVF of 10%, as shown in the inset.

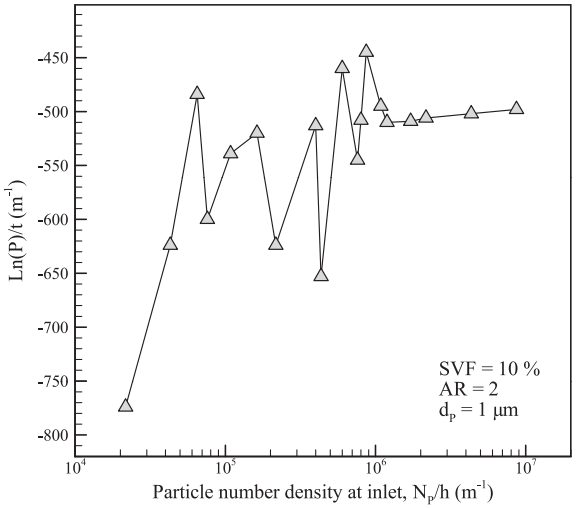

Fig. 7. Influence of number of particles injected at the inlet on the penetration prediction of a typical trilobal medium simulated in this study (SVF of 10% and aspect ratio of 2).

distance from the wall boundary. This has been done by continuously monitoring the distance between the particles' centers and fibers' surface during the trajectory tracking. If the particle's center of mass reaches a distance of $d_p/2$ away from a fiber, it will be counted as deposited. Note that for the Lagrangian particle tracking, symmetry boundary conditions act like a perfectly reflecting wall, i.e., particles colliding with the symmetry boundaries will be reflected without any loss of momentum.

Fig. 5a shows the particle concentration contour plot throughout the domain for a typical trilobal medium considered in this work. Red to blue represents normalized nanoparticle concentration from 1 to zero. Note that the nanoparticle concentration close to the fibers is almost zero indicating the particle deposition. Fig. 5b depicts the trajectory of particles' centers of mass for 0.5 μm particles in the same solution domain. For the sake of clarity, only a few particle trajectories are shown.

Our filter geometries were meshed with triangular cells in the filter zone and quadrilateral cells in the fluid entry zones. Depending on the fiber aspect ratio, 3,000,000 to 7,000,000 cells were used

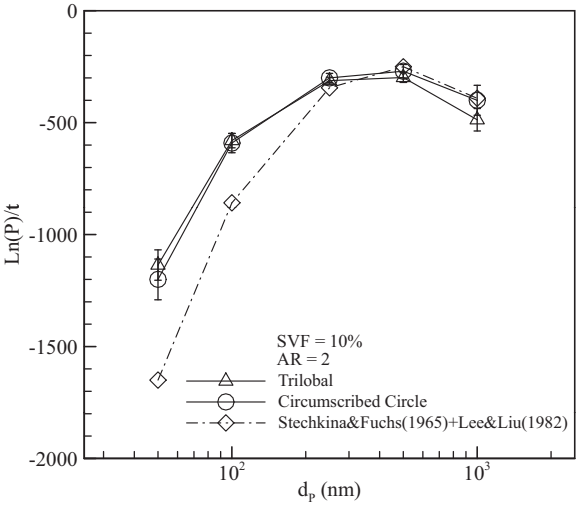

Fig. 8. Comparison between simulation results obtained for trilobal filters with SVF of 10% and aspect ratio of 2, and their equivalent circumscribed media. Predictions of the semi-empirical expressions of Stechkina and Fuchs [7] and Lee and Liu [8] are added for comparison.

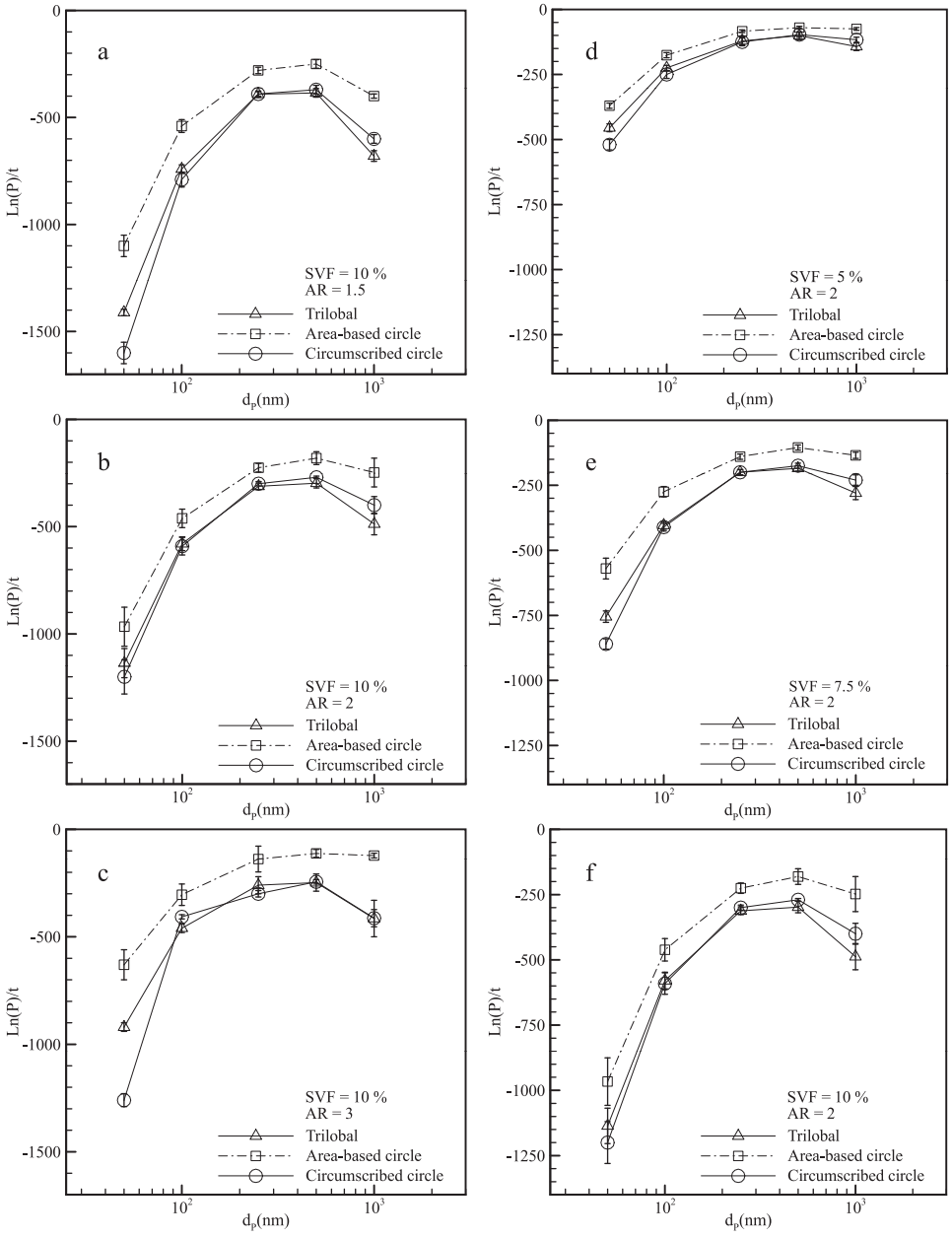

Fig. 9. Penetration per thickness for trilobal media and their equivalent area-based and circumscribed media at a constant SVF of 10% (a–c), and at a constant aspect ratio of 2 (d–f). Note that minor axis of the fibers' elliptical lobes is kept constant (2 μm) in the simulations reported in this paper, i.e., the fibers' cross-sectional area is not constant.

in the simulations presented in this paper. A larger numbers of cells are considered in simulations with greater aspect ratios to correctly resolve the flow field at shaper corners of high aspect ratio fibers.

To find out the minimum number of mesh points needed to conduct mesh-independent simulations, a single trilobal fiber was placed in the middle of a square 2-D domain. The sides of the square were chosen such that an SVF of 10% was achieved (see Fig. 6). The pressure drop caused by this single fiber was monitored as the number of mesh points per each lobe of the fiber was increased from 10 to 100. It can be seen that grid density has negligible effect on the pressure drop prediction for more than 80 grids per lobe.

To correctly predict the particle capture efficiency via interception and impaction, one must release a large number of particles in the flow domain to ensure that the results are independent of number of particles at inlet. Fig. 7 shows the influence of number of particles introduced at the inlet on the medium's collection efficiency using the Lagrangian method (Eq. (18)). The horizontal axis here is the number of particles per unit of length at the inlet, N_p/h. It can be seen that particle collection efficiency (due to interception and inertial impaction) is independent of the number density of the particles at the inlet beyond a value of about 2×10^6, and so we used this density for the particle injection at the inlet.

5. Results and discussion

As mentioned before, despite their wide spread applications, trilobal media have not been systematically studied in the literature. Unfortunately, there are no reliable experimental studies available in the literature that could be used here for our model validation. Therefore, we validate our simulation methodology by presenting a comparison between results of our simulations of circular media with the predictions of some of the available

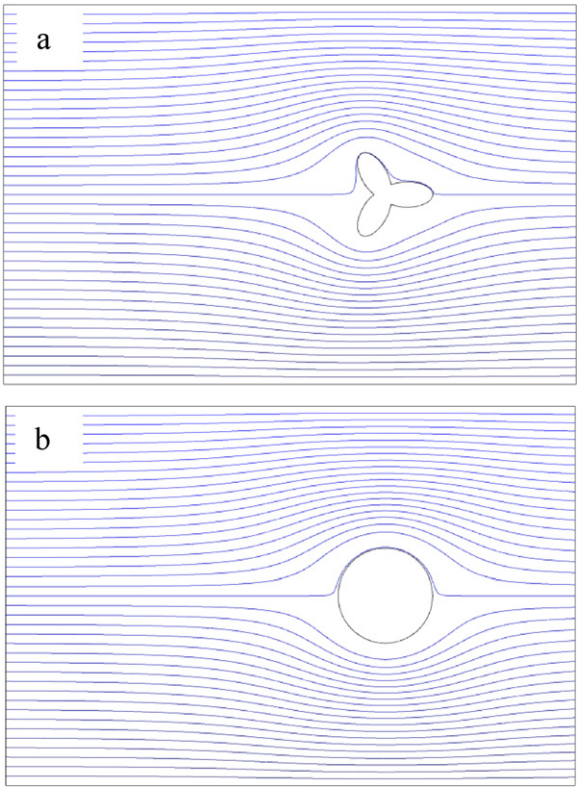

Fig. 10. Since the flow inside a fibrous medium is highly viscous (Re < 1) streamlines are deflected far before they reach the fiber. Deflection of the streamlines is mostly caused by the projected area of the fibers on a plane normal to the flow direction, rather than the exact shape of the fiber cross-section. It can be seen that the flow pattern around a trilobal fiber (a) and its circumscribed circle (b) are quite similar.

empirical/semi-empirical models that have been developed for media with circular fibers (see Section 2). Fig. 8 shows penetration per thickness through filter media with a SVF of 10% made up of circular fibers with a diameter of 14.9 μm along with the predictions of the expressions developed by Stechkina and Fuchs [7] and Lee and Liu [8] (Eqs. (3) and (4)). Good agreement between our modeling results and these empirical correlations is evident especially for particles >200 nm. In this figure, we also included our simulation results obtained for trilobal media with fibers having

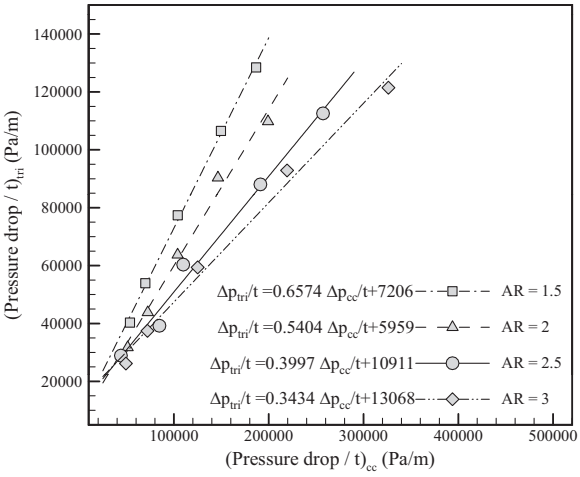

Fig. 11. Relationship between pressure drop of trilobal media and their equivalent circumscribed equivalents for a SVF of 10% and different aspect ratios of 1.5, 2, 2.5 and 3. Curve fitting equations are given for each case for convenience.

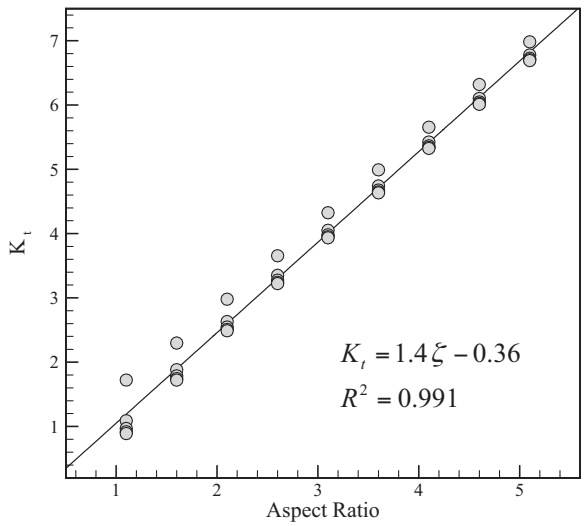

Fig. 12. Relationship between SVF of trilobal filters with different aspect ratios and different minor axis diameter, *b*, and those of their circumscribed equivalent media.

an aspect ratio of $\zeta = 2$ and a minor axis of $b = 2$ μm (resulting in a circumscribed diameter of 14.99 μm).

Fig. 9a–c shows the influence of the fiber's aspect ratio on penetration per thickness, $Ln(P)/t$ through trilobal media with a SVF of 10%. It can be seen that filters' penetration per thickness (for the range of particles considered) increases by increasing aspect ratio. Note that minor diameter of the fibers' elliptical lobes is kept constant (2 μm) in the simulations reported in this paper. Unlike the experimental work of Lamb and Costanza [2], the fibers' cross-sectional area is not kept constant in our study.

In Fig. 9d–f, one can see that penetration per thickness decreases by increasing the SVF, as expected. It can also be seen that there is good agreement between the results generated with circular fibers having a diameter obtained by using the trilobals' circumscribed diameter. In this figure, we also added the predictions obtained by using the aforementioned area-based equivalent circular diameters (see Section 2). It can be seen that the area-based equivalent diameter tends to overestimate particle penetration through the media, while the definition based on the circumscribed circle closely agree with the direct simulations of trilobal media. The idea of using the circumscribed circle was inspired by the fact that the flow inside a

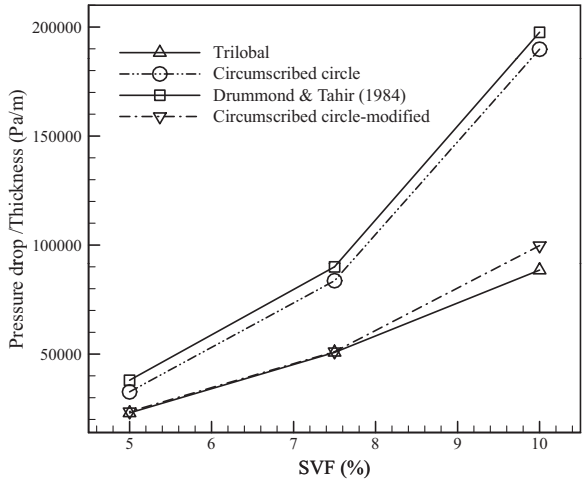

Fig. 13. Pressure drop per thickness for trilobal filters and their circumscribed equivalent media before and after pressure correction (see Fig. 11). Predictions or the well-known expression of Drummond and Tahir [6], obtained for circular media, are also added for validation.

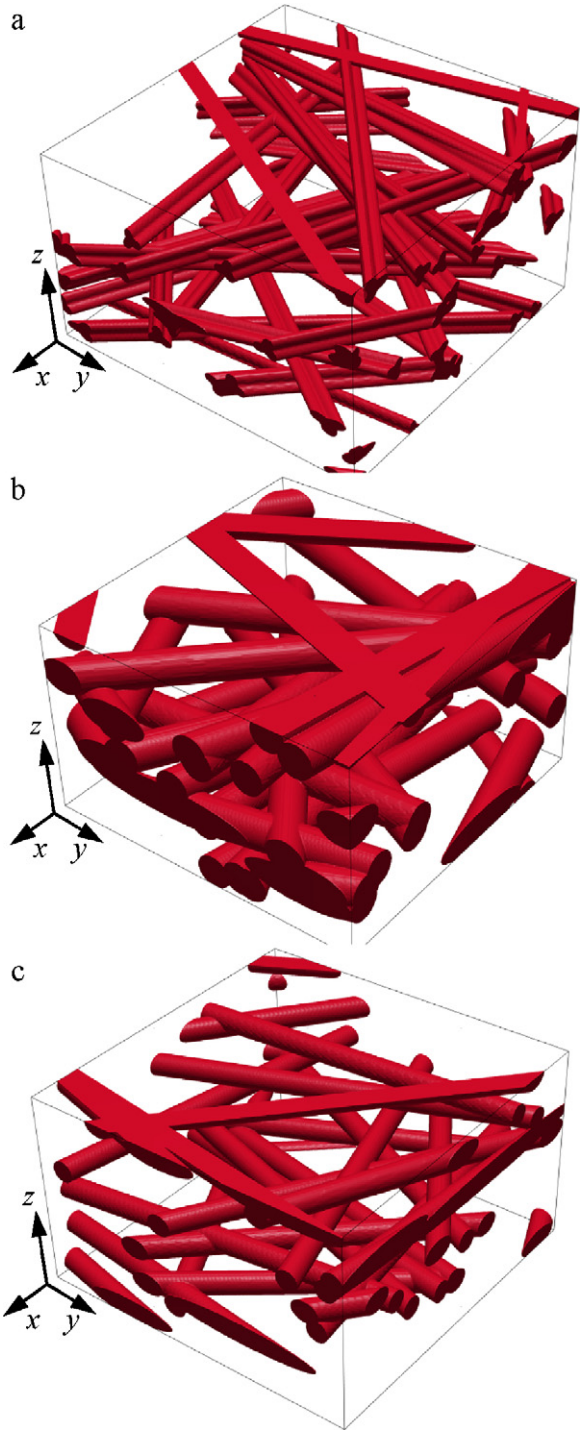

Fig. 14. Examples of three dimensional fibrous media generated for modeling pressure drop and collection efficiency in trilobal media fibers with an aspect ratio of 1.5 and an SVF of 10% (a), and their circumscribed (b) and area-based equivalent media (c).

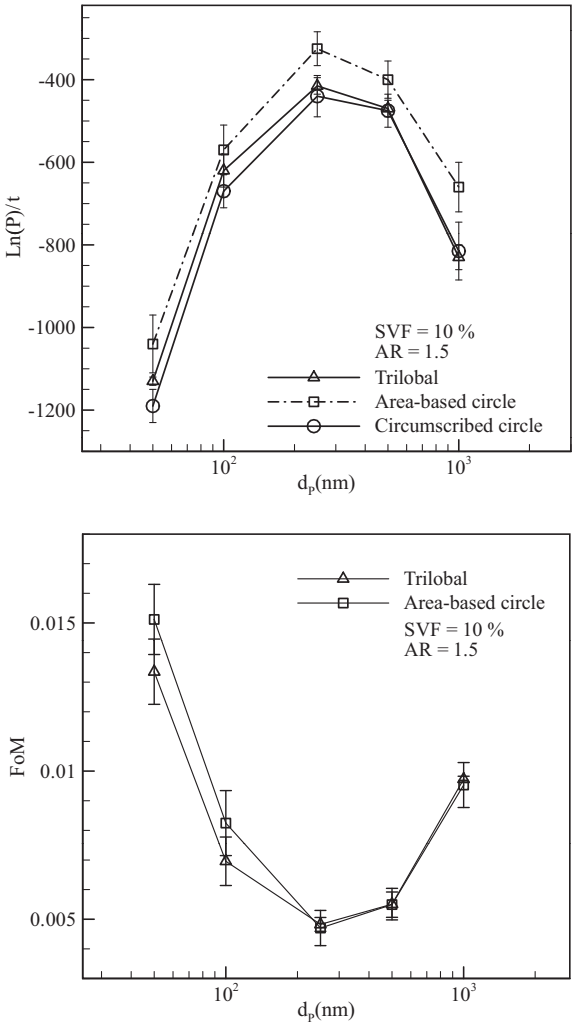

Fig. 15. Penetration per thickness calculated for the media shown in Fig. 14. Except for the case of area-based equivalent media, each simulation has been repeated three times.

fibrous medium is highly viscous (Re < 1) (i.e., Stokes flow regime), and the presence of an obstacle (whether trilobal or circular) is sensed by the fluid particles (as well as the solid nanoparticles) far upstream of the fiber (see Fig. 10). Therefore, streamlines are deflected far before they are close to the fiber. Deflection of the streamlines is mostly caused by the projected area of the fibers on a plane normal to the flow direction, rather than the exact shape of the fiber cross-section, and so is not very sensitive to the height or width of the lobes (note that the inertial effects are negligible for submicron particles, and they tend to follow their streamlines). Therefore, a fiber's collection efficiency is also not very sensitive to the lobe's geometry as the air in the grooves between the lobes seems to remain almost motionless, i.e., acting like a solid object against the flow.

The results shown in Fig. 9 indicate that diameter of the circumscribed circle of a trilobal fiber can effectively be used to predict collection efficiency of trilobal filters. It should be noted, however, that using this diameter, SVF of the media increases drastically. The new SVF helps achieve good predictions for collection efficiency; however, it results in wrong pressure drop estimates. To solve this problem, we simulated a series of trilobal single fibers in domains similar to the one shown in Fig. 6, and calculated the their pressure drops for different SVFs of 5, 6, 7.5, 9 and 10 percent and different aspect ratios of 1.5, 2, 2.5 and 3. These simulations were then repeated for the circumscribed equivalent fiber of each trilobal fiber for comparison purposes (see Fig. 11). In this figure, each line represents the relationship between pressure drop per thickness of trilobal filters and their equivalent circumscribed media. Fig. 11 can be used to predict the pressure drop of a trilobal medium, $(\Delta p/t)_{tri}$, using the pressure drop value of its equivalent circumscribed medium, $(\Delta p/t)_{cc}$, obtained with equations given in Section 2. For the sake of convenience, we also presented an equation for each line shown in Fig. 11. Note that to calculate $(\Delta p/t)_{cc}$, one needs

Table 1
Pressure drop of the media shown in Fig. 14. Prediction of the empirical correlation of Davies [31], obtained for media with circular fibers, is also added for validation.

3-D SVF = 10%	Trilobal	Circumscribed	Area-based	Davies [31]	Eqs. in Fig. 10
$\Delta P_{ave.}/t$ (kPa/m)	84.33	109.55	81.11	106.55	78
Std. dev.	6.67	16.67	2.78	–	–

to know the SVF of the equivalent circumscribed media. Assuming K_t to be the ratio of the SVF of the equivalent medium to that of the original trilobal media, we have:

$$K_t = \frac{\alpha_{cc}}{\alpha_{tri}} \tag{19}$$

where α_{tri} and α_{cc} are the SVF of media made of trilobal and circumscribed circles, respectively. In general, $K_t = K_t(\zeta, b)$, where $\zeta = a/b$ is the fiber aspect ratio. We calculated K_t for different values of $1 < b < 5$ micron and $1 < \zeta < 5$, and plotted the results in Fig. 12. It can be seen that dependence on b is quite negligible in comparison to that on the aspect ratio. This allows us to neglect the dependence on b and develop an easy expression for $K_t = K_t(\zeta)$, as follows:

$$K_t = 1.4\zeta - 0.36 \tag{20}$$

This equation can be used to calculate SVF of the circumscribed circle equivalent media of each trilobal filter.

In Fig. 13, we compare pressure drop per thickness of trilobal media and their equivalent circumscribed media as they were obtained from our CFD simulations. The media considered here have an aspect ratio of 2, a minor elliptical axis of $b = 2$ μm, and three different SVFs of 5, 7.5, and 10 percent. As explained earlier, pressure drop of the equivalent media is much higher than that of the actual trilobal filters. These pressure drop values are then corrected using the relationships given in Fig. 11 and added to Fig. 13. It can be seen that corrected pressure drop values are in good agreement with the values obtained for the trilobal media. In this figure we also included the predictions of the analytical model of Drummond and Tahir [6] for the equivalent circumscribed media. The good agreement between our simulation results and the well-known model of Drummond and Tahir [6] validates the accuracy of the simulations.

6. Test case: performance of 3-D filter media with AR = 1.5, SVF = 10%

This section is intended to examine whether or not equations and conclusions obtained from our 2-D simulations (Section 6) are valid for real 3-D filters. In the absence of reliable experimental data, we use 3-D virtual fibrous structures, as they more realistically represent the microstructure of a real filter medium. In our previous studies, we have demonstrated that 3-D simulations can be used to accurately predict the performance of a fibrous medium (see [22–25] for more information). Three-dimensional simulations, however, require extensive computing resources, and so are not suitable for extensive parameter study. Here, we use 3-D simulations for validation purposes only. To do so, we generate a few 3-D fibrous media using the Geodict CFD code and calculate their pressure drop and collection efficiencies. We then use our circumscribed equivalent media to predict these results. GeoDict is a voxel-based code developed by Fraunhofer ITWM, and validated in many recent publications by our group and others [26–30]. Our previous voxel size independence has revealed that consistent results can be obtained from GeoDict by using 15 or more voxels per fiber diameter. Here, we compare performance of trilobal media with that of their circumscribed and area-based equivalent structures (see Fig. 14). Collection efficiencies of these media are compared with one another in Fig. 15. It can be seen that circumscribed equivalent media, unlike the area-base model, can be used to predict efficiency of trilobal media with acceptable accuracy.

Table 1 presents pressure drop per thickness of media shown in Fig. 15. We also added the empirical correlation of Davies [31] for comparison. It can again be seen that our circumscribed circle equivalent model together wit this correction factor can be used to predict the pressure drop of a trilobal medium.

7. Conclusion

In this paper, for the first time we established a definition for an equivalent circular fiber that can be used with the traditional filtration correlations (developed for filters with circular fibers) for predicting collection efficiency of filters made of trilobal fibers. Our study was conducted in 2-D simulation domains, and due to the lack of suitable experimental data, validated via 3-D realistic simulations in which fibers random orientations were taken into account. We demonstrated that the circumscribed circle of trilobal fibers can be used with the existing traditional empirical/semi-empirical correlations to predict the performance of a trilobal filter medium. We believe that the information presented in this paper can be used by the manufacturers to predict and optimize the performance of their media, and help in reducing the experimental trials before the actual production process.

Acknowledgments

The current work is supported by the Nonwovens Cooperative Research Center (NCRC). Their support is gratefully acknowledged.

References

[1] Y. Watanabe, H. Sato, Y. Hirai, I.S. Kim, S. Hinata, J. Kim, Novel method to evaluate the net wear volume of bag-filter by fly ash, J. Hazard. Mater. 161 (2009) 775–780.
[2] G.E.R. Lamb, P.A. Costanza, Influences of fiber geometry on the performance of non-woven air filters: 3. cross-sectional shape, Text. Res. J. 50 (6) (1980) 362–370.
[3] J.R. Sanchez, J.M. Rodriguez, A. Alvaro, A.M. Estevez, The capture of fly ash particles using circular and noncircular cross-section fabric filters, Environ. Prog. 26 (1) (2007) 50–58.
[4] P.C. Raynor, S.W. Kim, CFD modeling of filter fibers with non-circular cross sections, in: AAAR Conference, Atlanta, 2004.
[5] K.R. Spurny, Advances in Aerosol Filtration, Lewis Publisher, CRC Press LLC, 1998.
[6] J.E. Drummond, M.I. Tahir, Laminar viscous flow through regular arrays of parallel solid cylinders, Int. J. Multiphas. Flow 10 (3) (1984) 515–540.
[7] I.B. Stechkina, N.A. Fuchs, Studies on fibrous aerosol filters-I. Calculation of diffusional deposition of aerosol in fibrous filters, Ann. Occup. Hyg. 9 (1965) 59–64.
[8] K.W. Lee, B.Y.H. Liu, Theoretical study of aerosol filtration by fibrous filters, Aerosol Sci. Technol. 1 (1982) 147–161.
[9] I.B. Stechkina, A.A. Kirsh, N.A. Fuchs, Investigation of the fibrous filters for aerosols calculation of aerosol deposition in model filters in region of maximum particle breakthrough, Colloid J. 31 (1) (1969) 97.
[10] R.C. Brown, Air Filtration, Pergamon Press, 1993.
[11] L.L. Xue, K.B. Koller, Q. Gao, US Patent 6,907,885 B2 (2005).
[12] S.K. Friedlander, Smoke, Dust, and Haze: Fundamentals of Aerosol Dynamics, 2nd ed., Oxford University Press, 2000.
[13] A. Li, G. Ahmadi, Dispersion and deposition of spherical-particles from point sources in a turbulent chemical flow, Aerosol Sci. Technol. 16 (4) (1992) 209–226.
[14] Q. Wang, B. Maze, H.V. Tafreshi, B. Pourdeyhimi, A case study of simulating submicron aerosol filtration via spun-bonded filter media, Chem. Eng. Sci. 61 (2006) 4871.
[15] Q. Wang, B. Maze, H.V. Tafreshi, B. Pourdeyhimi, Simulating through-plane permeability of fibrous materials having different fiber lengths, Model. Simul. Mater. Sci. 15 (2007) 855–868.

[16] S.A. Hosseini, H.V. Tafreshi, 3-D simulation of particle filtration in electrospun nanofibrous filters, Powder Technol. 201 (2010) 153–160.
[17] J. Wang, D.Y.H. Pui, Filtration of aerosol particles by elliptical fibers: a numerical study, J. Nanopart. Res. 11 (1) (2009) 185–196.
[18] P.C. Raynor, Single-fiber interception efficiency for elliptical fibers, Aerosol Sci. Technol. 42 (2008) 357–368.
[19] B.D. Regan, P.C. Raynor, Single-fiber diffusion efficiency for elliptical fibers, Aerosol Sci. Technol. 43 (6) (2009) 533–543.
[20] S. Fotovati, H.V. Tafreshi, A. Ashari, S.A. Hosseini, B. Pourdeyhimi, Analytical expressions for predicting capture efficiency of bimodal fibrous filters, J. Aerosol Sci. 41 (2010) 295.
[21] S.A. Hosseini, H.V. Tafreshi, Modeling particle filtration in 2-D disordered domains: a comparison with cell models, Sep. Purif. Technol. 74 (2010) 160–169.
[22] Q. Wang, B. Maze, H.V. Tafreshi, B. Pourdeyhimi, A Note on permeability simulation of multifilament woven fabrics, Chem. Eng. Sci. 61 (2006) 8085.
[23] S. Jaganathan, H.V. Tafreshi, B. Pourdeyhimi, A case study of realistic two-scale modeling of water permeability in fibrous media, Sep. Sci. Technol. 43 (2008) 1901.
[24] M.A. Tahir, H.V. Tafreshi, Influence of fiber orientation on the transverse permeability of fibrous media, Phys. Fluids 21 (2009) 083604.
[25] S.A. Hosseini, H.V. Tafreshi, Modeling permeability of 3-D nanofiber Media in slip flow regime, Chem. Eng. Sci. 65 (2010) 2249–2254.
[26] H.V. Tafreshi, M.S. Rahman, S. Jaganathan, Q. Wang, B. Pourdeyhimi, Analytical expressions for predicting permeability of bimodal fibrous porous media, Chem. Eng. Sci. 64 (2009) 1154–1159.
[27] N. Zamel, X. Li, J. Shen, Correlation for the effective gas diffusion coefficient in carbon paper diffusion media, Energy Fuel 23 (2009) 6070–6078.
[28] H. Thoemen, T. Walther, A. Wiegmann, 3D simulation of macroscopic heat and mass transfer properties from the microstructure of wood fiber networks, Compos. Sci. Technol. 68 (3–4) (2008) 608–616.
[29] V.P. Schulz, J. Becker, A. Wiegmann, P.P. Mukherjee, C. Wang, Modeling of two-phase behavior in the gas diffusion medium of PEFCS via full morphology approach, J. Electrochem. Soc. 154 (4) (2007) 419–426.
[30] K. Schladitz, S. Peters, D. Reinel-Bitzer, A. Wiegmann, J. Ohser, Design of acoustic trim based on geometric modeling and flow simulation for non-woven, Comp. Mater. Sci. 38 (1) (2006) 56–66.
[31] C.N. Davies, Air Filtration, Academic Press, London, 1973.